Available online at www.sciencedirect.com
SCIENCE DIRECT®
Optics Communications 245 (2005) 67–73
OPTICS COMMUNICATIONS
www.elsevier.com/locate/optcom

Highly polarization-sensitive thick gratings for a holographic Stokesmeter

M.S. Shahriar, J.T. Shen *, M.A. Hall, Renu Tripathi, Jong Kwon Lee, Alex Heifetz

Department of Electrical and Computer Engineering, Northwestern University, 2145 N Sheridan Road, Evanston, IL 60208, USA

Received 1 June 2004; received in revised form 27 September 2004; accepted 1 October 2004

Abstract

A holographic Stokesmeter has the potential to be useful in high-speed polarization imaging applications. Highly polarization-sensitive gratings are an important component in a robust holographic Stokesmeter. We demonstrate a set of individual holographic gratings in a thick substrate displaying a high contrast in diffraction efficiency as a function of the polarization of the read beam. We confirm that the observed dependence is consistent with the coupled-wave analysis of such gratings. In addition, we performed a numerical analysis of the noise tolerance of such a Stokesmeter, and suggest a heterodyne architecture to further enhance signal-to-noise ratio.

Keywords: Holography; Volume holographic gratings; Polarimetry

Polarization imaging [1–3] can discriminate a target from its background in situations where conventional imaging methods fail. Identifying the components of the polarization of the light reflected from the target allows one to construct an image that corresponds to the target's unique polarimetric signature. This is useful in applications ranging from target recognition to vegetation mapping [4–7]. Identifying the Stokes vector of the scattered light completely characterizes the polarization of the light [8]. Current architectures for such a Stokesmeter include mechanical quarter-wave plate/linear polarizer combinations, photo-detectors with polarization filtering gratings etched onto the pixels, and liquid crystal variable retarders [9–13]. The mechanical system is limited by the fact that it must rotate the angle between the wave-plate and polarizer before

* Corresponding author. Tel.: +1 8474917308; fax: +1 8474914455.
E-mail address: jshen@ece.northwestern.edu (J.T. Shen).

0030-4018/$ - see front matter © 2004 Elsevier B.V. All rights reserved.
doi:10.1016/j.optcom.2004.10.002

determining each Stokes parameter. Polarization gratings cannot currently resolve the full Stokes vector. The liquid crystal (LC) variable retarder system is analogous to the mechanical waveplate/polarizer system with an LC display replacing the waveplates. The process is still sequential and the time required to reset the display limits the device to ~10 Hz. Systems based on the waveplate/polarizer architecture that split the beam into four parts and calculate the parameters in parallel require four times as many optical components as a system based on a single holographic substrate, beamsplitter, and waveplate.

Grating based polarimeters have been proposed and demonstrated for use in spectroscopic ellipsometry applications by Azzam and co-workers [14,15] and by Todorov and Nikolova [16]. These types of polarimeters are based on measuring the intensity of multiple orders of diffraction from a thin grating (two such gratings in the case of Todorov and Nikolova). These devices also utilize the polarization properties of gratings, however, several key differences exist. First, these polarimeters are based on measuring the intensity of multiple orders of diffraction from a thin grating. Because only four orders are needed for measurement, any energy diffracted into other orders is wasted. In our case of the thick holographic Stokesmeter, it is simple to design the hologram in such a way as to divide the incident power into the diffracted beams with no energy being directed into unused orders. Another difference between thick and thin gratings is evident in their spectral selectivity. Thin gratings have a large spectral bandwidth, so for polychromatic sources, each diffracted order will have an angular spread associated with it. By contrast, the thick hologram acts as a natural spectral filter, allowing only a very narrow range of wavelengths (typically much less than 1 nm) [17]. This difference is important for constructing a polarimetric image. For the thin grating Stokesmeter, because of the angular spread, at a given detector point there will be a signal due to one wavelength at the expected diffraction order plus some signal due to a different wavelength from a neighboring diffraction order. This will present a noisy image and will be difficult to overcome. Our thick holographic Stokesmeter will not have this problem, and thus will be more suited to polarimetric imaging.

A holographic Stokesmeter can be used to resolve all four Stokes components in parallel and at a high speed [18]. For a typical thick holographic grating, the response time of the device can be on the order of 10 ps. This removes the device as the bottleneck in the imaging system and instead the desired signal-to-noise ratio and detector parameters set the upper limit on the speed of the polarimeter. The details of this Stokesmeter are presented in [18]. Here, it is instructive to recall briefly the essential features (see Fig. 1).

The architecture for a holographic Stokesmeter utilizes the polarization-dependence of thick holographic gratings to resolve the components of the Stokes vector. Four gratings are used with two angles of rotation. The scattered light is split and half is diffracted from the first two gratings while the other half passes through a quarter-wave plate before diffracting from the remaining two gratings. A Mueller matrix analysis of the architecture leads to a measurement matrix involving the diffraction efficiencies for s- and p-polarized light of the four gratings (weighted by the appropriate Fresnel transmittances) and the rotation angles of the gratings

$$\begin{bmatrix} I_{t1} \\ I_{t2} \\ \mathrm{I}_{t3} \\ \mathrm{I}_{t4} \end{bmatrix} = \begin{bmatrix} A_1 + B_1 & (A_1 - B_1)\cos(2\gamma_1) & (A_1 - B_1)\sin(2\gamma_1) & 0 \\ A_2 + B_2 & (A_2 - B_2)\cos(2\gamma_2) & (A_2 - B_2)\sin(2\gamma_2) & 0 \\ A_3 + B_3 & (A_3 - B_3)\cos(2\gamma_1) & 0 & -(A_3 - B_3)\sin(2\gamma_1) \\ A_4 + B_4 & (A_4 - B_4)\cos(2\gamma_2) & 0 & -(A_4 - B_4)\sin(2\gamma_2) \end{bmatrix} \begin{bmatrix} I \\ Q \\ U \\ V \end{bmatrix}, \quad (1)$$

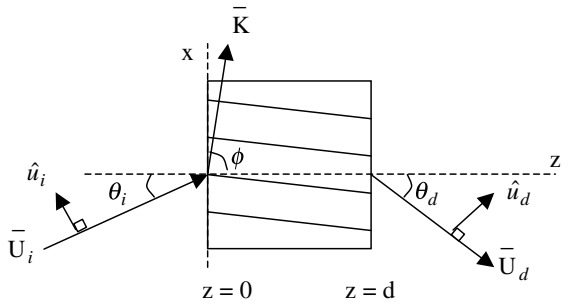

Fig. 1. Diffraction from a thick grating.

where the coefficients A_i and B_i depend on perpendicular and parallel components of the diffraction efficiency for the ith grating and γ_j are the angles of rotation. I_{t1-4} are the four measured intensities that are required and I, Q, U and V are the four Stokes components to be determined. In order for the matrix in (1) to be well-conditioned [19,20], the diffraction efficiencies of the four gratings need to be chosen properly along with the other parameters. Given that the coefficients of the matrix in (1) depend on polarization-sensitive diffraction it can be seen that in order to design a robust system, one must be able to control the amount of diffraction for each polarization very carefully. For example, it may be desirable for A–B to be a large negative quantity, which requires a grating that ideally diffracts only p-polarized light. One might also require A–B to be a large positive quantity, requiring a grating that ideally diffracts only s-polarized light. We demonstrate preliminary results for such gratings and show that the polarization dependence of these gratings can be accurately described by coupled-wave analysis.

The derivation of the coupled-wave equations for arbitrary polarization is straightforward and can be found in [17]. Here, we present the result

$$\begin{aligned}\cos\theta_i \frac{\partial}{\partial z} U_i &= -i\kappa(\hat{u}_i \cdot \hat{u}_d) U_d,\\ \cos\theta_d \frac{\partial}{\partial z} U_d &= -i\kappa(\hat{u}_i \cdot \hat{u}_d) U_i.\end{aligned} \tag{2}$$

Note that for $\hat{u}_i \cdot \hat{u}_d = 1$, the equations reduce to the case of perpendicular polarization. The diffraction efficiency for general polarization follows from Eq. (2):

$$\eta = \sin^2\left(\kappa(\hat{u}_i \cdot \hat{u}_d)\frac{d}{\sqrt{\cos\theta_i \cos\theta_d}}\right). \tag{3}$$

For the case of parallel polarization the dot product $\hat{u}_i \cdot \hat{u}_d = -\cos(2(\theta_i - \phi))$, and the equations for the diffraction efficiency of each polarization are as follows:

$$\begin{aligned}\eta_\perp &= \sin^2\left(\frac{\pi n'}{\lambda}\frac{d}{\sqrt{\cos\theta_i \cos\theta_d}}\right),\\ \eta_\parallel &= \sin^2\left(\frac{\pi n'}{\lambda}\frac{d}{\sqrt{\cos\theta_i \cos\theta_d}}\cos\left(2(\theta_i - \phi)\right)\right).\end{aligned} \tag{4}$$

One can observe what can be considered a holographic Brewster angle for geometries such that $\theta_i - \phi = 45°$.

Studies of the polarization dependence of the diffraction efficiency have been carried out for the case of achieving elimination of one unwanted polarization, using the holographic Brewster angle method, for the purpose of creating holographic optical elements [21,22]. We are interested in establishing the precision with which the observed polarization diffraction contrast matches the analytic theory. In particular, this requires an indirect determination of the index modulation amplitude from the diffraction efficiency of one polarization. This value is then used to predict the diffraction efficiency at the other polarization, in order to compare with the experimental value. Finally, this is the first time where the polarization contrast gratings have been made in the Memplex™ material, which is a key candidate for realizing the Stokesmeter.

The Memplex material we use is a dye-doped photopolymer with an index of refraction of 1.482 and a sample thickness of 2 mm. Given the index of this material, it is not possible to achieve the required $\theta_i - \phi = 45°$ condition using beams incident on the same surface. However, if one were to use a cubic geometry the condition is easily achievable. The gratings used here were written at 532 nm with writing angles of 52.5° and 57° to produce a slanted grating. Reading was done at the same wavelength and at 57°. Six individual gratings were written using different exposure times. The diffraction efficiency was then measured for various angles of the polarization of the incident read beam. The readout setup is shown in Fig. 2.

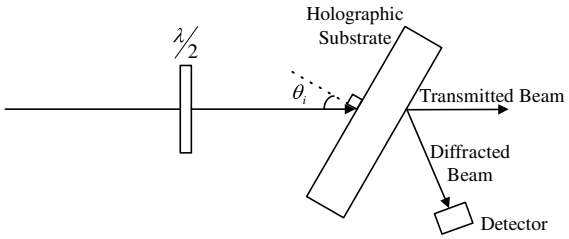

Fig. 2. Readout setup.

Theoretical results were calculated using Eq. (4). The value of n' was calculated using Eq. (4) with measured values of the diffraction efficiency and compensating for Fresnel reflection loss.

The gratings were read at the Bragg angle, so the angles of the incident and diffracted beam are known and were used to determine Fresnel reflections. These reflections were taken into account and Eq. (4) was used to determine the theoretical diffraction efficiency. The theoretical and experimental results are plotted in Fig. 3 without using

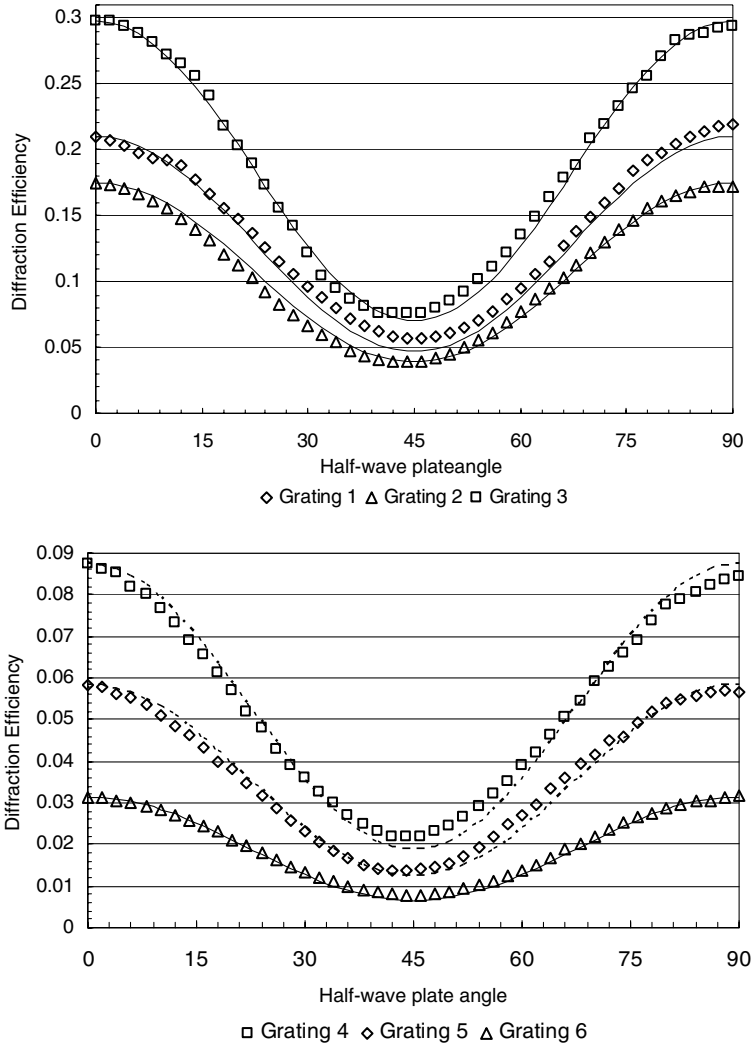

Fig. 3. Diffraction efficiency vs. polarization. 0° and 90° are s-polarized and 45° is p-polarized. Dashed line indicates theoretical calculations.

any free fitting parameter. Note that the experimental deviation from the coupled-wave theory is very small. These results also demonstrate a high degree of contrast in diffraction efficiency between the s- and p-polarizations, greater than 70% in some cases.

Two separate numerical simulations were performed in order to simulate the performance of the holographic Stokesmeter in the presence of noise. The first case considered the effect of additive white Gaussian noise (AWGN) added to the four intensity measurements. The measurement matrix is assumed to be known without error. The second case considers no noise in the intensity measurements, but includes noise in the measurement matrix itself. For each of these cases a variety of Stokes vectors were tested. Shown here are the results for the Stokes vector $[1 \quad -0.6 \quad 0 \quad 0.8]$ averaged over 200 runs. Percent error is plotted versus the contrast ratio of the gratings. The grating parameters used in the simulation were in favor of stronger diffraction of perpendicular polarization for the first and fourth grating and in favor of stronger diffraction of parallel polarization for the second and third grating. The rotation angles used were 5° and 40°. Using these grating parameters leads to an improvement of the measurement matrix, however, these parameters do not necessarily represent the optimal set. A more exhaustive search through the entire parameter space is required to fully optimize the measurement matrix. The variance of the noise used was −25, −30, −35 and −40 dB compared to a maximum normalized intensity of 1.

The results for case one are shown in Fig. 4. We see from the figure that as the contrast ratio increases, the average percent error decreases, with limiting gains in the improvement past 50% contrast. These error results are specific to the chosen input Stokes vector, but the general trend is the same for an arbitrary input.

The results for case two are shown in Fig. 5. This case shows the same trend of decreasing error as the contrast ratio increases. Note the unusually large error for contrast ratio values less than 50% in this case. This is due to the fact that the noise is added to the measurement matrix in this scenario, and for average noise values that are larger than the difference between the parallel and perpendicular polarization components of the diffraction efficiency, the sign of the terms $A_i + B_i$ in Eq. (1) will change. This can lead to very large errors in the calculation. As the contrast ratio increases, this effect lessens and the percent error rates approach normal values.

As we can see from the data in Figs. 4 and 5, for contrast ratios of greater than 50%, a relatively noise-tolerant holographic Stokesmeter can be

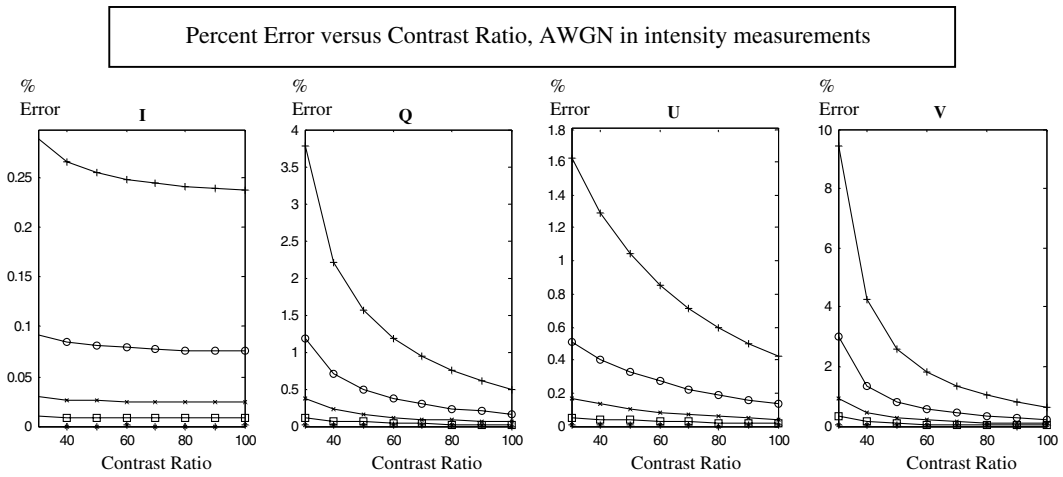

Fig. 4. Percent error plotted versus contrast ratio for each Stokes parameter for the case of AWGN in the intensity measurements. The separate lines in each graph represent the different noise levels: + = −25 dB; ○ = −30 dB; × = −35 dB; □ = −40 dB; ∗ = no noise.

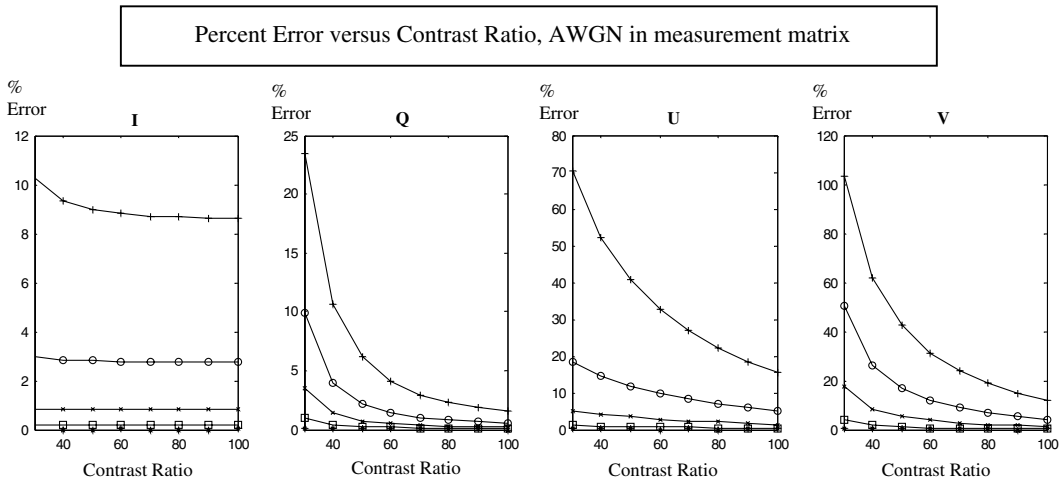

Fig. 5. Percent error plotted versus contrast ratio for each Stokes parameter for the case of AWGN in the measurement matrix. The separate lines in each graph represent the different noise levels: + = −25 dB; ○ = −30 dB; × = −35 dB; □ = −40 dB; ∗ = no noise.

constructed depending on the noise level and the desired percent error. The gratings shown here demonstrated a contrast ratio of above 70%, indicating that they will be adequate for use in constructing a preliminary version of the holographic Stokesmeter.

If a further improvement in signal-to-noise ratio is desired, a heterodyne receiver configuration can be easily added to the holographic Stokesmeter architecture. This architecture is illustrated in Fig. 6. The four diffracted beams represent the four intensities to be measured. These beams are mixed with a strong local oscillator using polarizing beamsplitters. The local oscillator is chosen to be linearly polarized at 45° so that both the perpendicular and the parallel components of the diffracted light will be mixed with the local oscillator evenly. Each of the eight beams is then sent through a standard heterodyne receiver architecture and the value of the perpendicular and parallel components of each of the four diffracted beams is recovered. These can then be used in conjunction with the measurement matrix to determine the four Stokes parameters. The heterodyne architecture has the advantage of helping to overcome the system noise and improve the signal-to-noise ratio by providing additional input intensity.

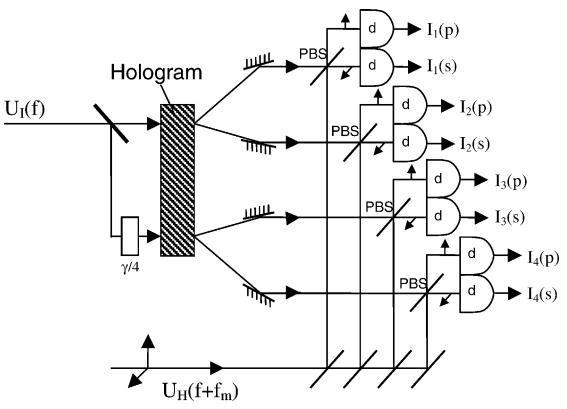

Fig. 6. Heterodyne receiver for holographic Stokesmeter.

We have demonstrated that highly polarization-sensitive holographic gratings required for a holographic Stokesmeter can be made. These gratings can be accurately described by coupled-wave analysis. We have performed a numerical analysis of the noise tolerance of the Stokesmeter, and the gratings demonstrated will allow the construction of a preliminary holographic Stokesmeter. The use of a heterodyne receiver architecture can lead to additional gains in the signal-to-noise ratio.

References

[1] J.L. Pezzaniti, R.A. Chipman, Opt. Eng. 34 (1995) 1558.
[2] K.P. Bishop, H.D. McIntire, M.P. Fetrow, L. McMackin, Proc. SPIE 3699 (1999) 49.

[3] G.P. Nordin, J.T. Meier, P.C. Deguzman, M.W. Jones, J. Opt. Soc. Am. A 16 (1999) 1168.
[4] L.J. Denes, M. Gottlieb, B. Kaminsky, D. Huber, Proc. SPIE 3240 (1998) 8.
[5] T. Nee, S.F. Nee, Proc. SPIE 2469 (1995) 231.
[6] W.G. Egan, Proc. SPIE 1747 (1992) 2.
[7] P.J. Curran, Remote Sens. Environ. 12 (1982) 491.
[8] A. Gerrard, J.M. Burch, Introduction to Matrix Methods for Optics, Dover Publications, New York, 1974.
[9] R.M.A. Azzam, Opt. Lett. 2 (1977) 148.
[10] D.H. Goldstein, Appl. Opt. 31 (1992) 6676.
[11] J.L. Pezzaniti, R.A. Chipman, Proc. SPIE 2297 (1994) 468.
[12] J.S. Tyo, T.S. Turner Jr., Proc. SPIE 3753 (1999) 214.
[13] J.M. Bueno, P. Artal, Opt. Lett. 24 (1999) 64.
[14] R.M.A. Azzam, K.A. Giardina, JOSA A 10 (6) (1993) 1190.
[15] A. Krishnan, S. Hampton, J. Rix, B. Taylor, R.M.A. Azzam, Appl. Opt. 42 (7) (2003) 1216.
[16] T. Todorov, L. Nikolova, Opt. Lett. 17 (1992) 358.
[17] H. Kogelnik, Bell Syst. Tech. J . 48 (1969) 2909.
[18] M.S. Shahriar, J.T. Shen, R. Tripathi, M. Kleinschmitt, T. Nee, S.F. Nee, Opt. Lett. 29 (2004) 3.
[19] A. Ambirajan, D.C. Look, Opt. Eng. 34 (1995) 1651.
[20] D.S. Sabatke, A.M. Locke, M.R. Descour, W.C. Sweatt, J.P. Garcia, E.L. Dereniak, S.A. Kemme, G.S. Phillips, Proc. SPIE 4133 (2000) 75.
[21] S. Habraken, Y. Renotte, St. Roose, E. Stijns, Y. Lion, Appl. Opt. 34 (19) (1995) 3596.
[22] C. Carre, S. Habraken, St. Roose, Opt. Lett. 18 (9) (1993) 738.